

# Lead Evaluation of Tetrahydroquinolines as Nonsteroidal Selective Androgen Receptor Modulators for the Treatment of Osteoporosis

Naoya Nagata,\* Kazuyuki Furuya, Nao Oguro, Daisuke Nishiyama, Kentaro Kawai, Noriko Yamamoto, Yuki Ohyabu, Masahiro Satsukawa, and Motonori Miyakawa<sup>[a]</sup>

Tetrahydroquinoline (THQ) was deemed to be a suitable scaffold for our nonsteroidal selective androgen receptor modulator (SARM) concept. We adapted the strategy of switching the antagonist function of cyano-group-containing THQ (CN-THQ) to the agonist function and optimized CN-THQ as an orally available drug candidate with suitable pharmacological and ADME profiles. Based on binding mode analyses and synthetic accessibility, we designed and synthesized a compound that possesses a *para*-substituted aromatic ring attached through an amide linker. The long-tail THQ derivative 6-acetamido-*N*-(2-(8-cyano-3a,4,5,9b-tetrahydro-3*H*-cyclopenta[*c*]quinolin-4-yl)-2-methylpropyl)nicotinamide (**1d**), which bears a *para*-acet-

amide-substituted aromatic group, showed an appropriate in vitro biological profile, as expected. We considered that the large conformational change at Trp741 of the androgen receptor (AR) and the hydrogen bond between **1d** and helix 12 of the AR could maintain the structure of the AR in its agonist form; indeed, **1d** displays strong AR agonistic activity. Furthermore, **1d** showed an appropriate in vivo profile for use as an orally available SARM, displaying clear tissue selectivity, with a separation between its desirable osteoanabolic effect on femoral bone mineral density and its undesirable virilizing effects on the uterus and clitoral gland in a female osteoporosis model.

## Introduction

Osteoporosis is a common, age-related bone disease that results from an imbalance between bone formation and bone resorption processes, leading to decreased bone mass and increased risk of fracture.<sup>[1]</sup> Calcium, vitamin D<sub>3</sub> supplementation, and bone resorption inhibitors such as bisphosphonates, estrogens, and selective estrogen receptor modulators (SERMs) are commonly used in the prevention and treatment of osteoporosis. Bisphosphonates and estrogens increase bone mineral density (BMD) by decreasing bone resorption. SERMs also increase BMD to the same extent as estrogen without affecting female sexual organs, such as the breasts and uterus. In contrast, androgens and parathyroid hormones (PTHs) are known to have positive effects on BMD by increasing bone formation.<sup>[2]</sup> Although one PTH (teriparatide, for example) is known as a bone-formation enhancer, its use requires subcutaneous injection for up to two years.<sup>[3]</sup>

The endogenous androgen, testosterone (TES), and its active metabolite, dihydrotestosterone (DHT), play important roles in the development and maintenance of the male phenotype, including the male reproductive system, muscles, bone, hair, larynx, and skin. Androgens bind to the androgen receptor (AR) and induce a conformational change at helix 12 (H12), converting the AR to its agonist form. The activated AR translocates to the nucleus and mediates the biological effects of an-

drogens. The major biological effects of androgens are classified into two categories: androgenic effects and anabolic effects. The androgenic effects include the development and maintenance of the male reproductive organs, secretory glands, and so on. The anabolic effects include the growth of muscles, bones, etc.

Steroidal AR ligands have been used therapeutically, but their use is limited by serious side effects toward reproductive organs (androgenic effects) and liver (hepatotoxicity). Therefore, nonsteroidal selective androgen receptor modulators (SARMs) are required to separate the anabolic effects from the androgenic effects.<sup>[4]</sup> Various SARMs have been identified in preclinical studies, but the mechanism underlying their tissue selectivity remains unclear.<sup>[5–7]</sup> Narayanan et al. proposed four mechanisms that may underlie the tissue selectivity of SARMs: 1) the role of 5 $\alpha$ -reductase, 2) the tissue-specific expression of co-regulators, 3) differences in the complexes that are formed by the AR in anabolic and androgenic tissues, and 4) the tissue-specific roles of intracellular signaling cascades.<sup>[7]</sup>

Co-crystallized ligand–protein structures have been used effectively to both understand the functional mechanisms of members of the nuclear receptor superfamily and for structure-based drug design (SBDD).<sup>[8]</sup> Various research groups have solved the co-crystal structures of their SARMs that possess agonistic activity toward wild-type AR and have been able to use their binding modes to design various therapeutic agents.<sup>[9–14]</sup> For example, Nique et al. used the co-crystal structure of diarylhydantoin in complex with AR for docking studies and managed to improve the oral bioavailability of diarylhydantoin by

[a] Dr. N. Nagata, Dr. K. Furuya, N. Oguro, D. Nishiyama, Dr. K. Kawai, N. Yamamoto, Y. Ohyabu, Dr. M. Satsukawa, Dr. M. Miyakawa  
Central Research Laboratories, Kaken Pharmaceutical Co. Ltd.  
14 Shinomiya, Minamikawara-cho, Yamashina, Kyoto 607-8042 (Japan)  
E-mail: nagata\_naoya@kaken.co.jp

introducing a hydroxymethyl group at the 4-position of the hydantoin scaffold.<sup>[13]</sup> Bohl et al. analyzed multiple co-crystal structures of diarylpropionamides with the AR and gained an understanding of the binding modes of diarylpropionamide derivatives.<sup>[9,10]</sup> GTx-007, a diarylpropionamide derivative, is known to be a SARM and is currently undergoing clinical investigation (Figure 1).<sup>[15,16]</sup> The binding mode of GTx-007 is distinct

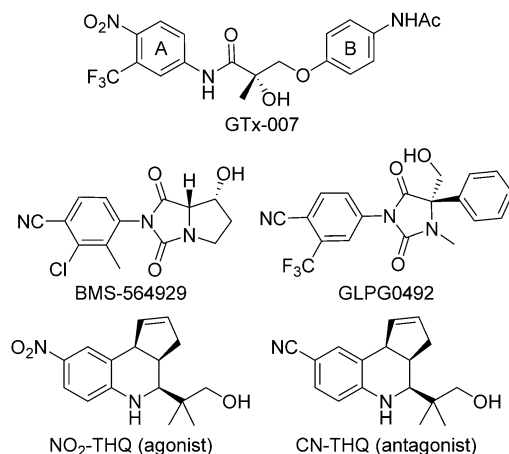


Figure 1. Nonsteroidal SARMs.

from that of other SARMs that display agonistic activity. Small AR agonists do not interact with Trp741 in helix 4 (H4), whereas the B ring of GTx-007 strongly interacts with the aromatic side chain of Trp741 in H4 and is stabilized through a  $\pi$ - $\pi$  interaction.<sup>[10]</sup> The stabilization of GTx-007 induces the folding of H12 into its agonist form, which is similar to that of known agonists.

We recently reported nitro-containing tetrahydroquinolines (NO<sub>2</sub>-THQs) as novel lead compounds of nonsteroidal SARMs and that they possess tissue-selective anabolic activities in both in vitro and in vivo studies.<sup>[17–19]</sup> These results validated THQ as a scaffold suitable for the development of our desired SARMs. In our lead-finding process, we demonstrated that THQ compounds change their behavior following subtle structural modifications; NO<sub>2</sub>-THQ acted as an agonist, while cyano-containing THQ (CN-THQ) acted as an antagonist. The strategy of switching an antagonist into an agonist has often succeeded for nonsteroidal SARMs, including

GTx-007, BMS-564929, and GLPG0492 (Figure 1).<sup>[9,12,20]</sup> We hypothesized that it might be possible to convert CN-THQ from an antagonist into an agonist while avoiding the potential risk of mutagenicity by the *para*-nitro aniline portion of NO<sub>2</sub>-THQ<sup>[21]</sup> and maintaining its tissue-selective anabolic activities. In our dynamic structural analyses, we found that the combination of the cyano and terminal hydroxy groups of CN-THQ results in the antagonistic activity of the AR.<sup>[22]</sup> Therefore, we postulated that replacement of the hydroxy group on CN-THQ with another functional group could be an essential step required to alter the activity of CN-THQ. Herein we describe the lead evaluation process of our THQ derivatives as SARMs.

## Results and Discussion

### Docking

For the SBDD of the new THQ derivatives, we first compared the key interactions between three different ligand-AR complexes (Figure 2a–c),<sup>[10,22,23]</sup> the shapes and volumes of the ligand binding pockets of two co-crystallized structures (Figure 3), and the 2D substructures of GTx-007 with CN-THQ.

In the DHT-AR complex (PDB ID: 1T7T),<sup>[22]</sup> DHT is stabilized by electrostatic interactions with the nearest neighboring polar atom of the hydrophilic residues Asn705, Gln711, Arg752, and Thr877 and by van der Waals (vdW) interactions with the surrounding hydrophobic residues Leu701, Leu704, Met742, Met745, Phe764, and Leu703 (Figure 2a). The 3-carbonyl group is stabilized through Coulombic interactions with the amide

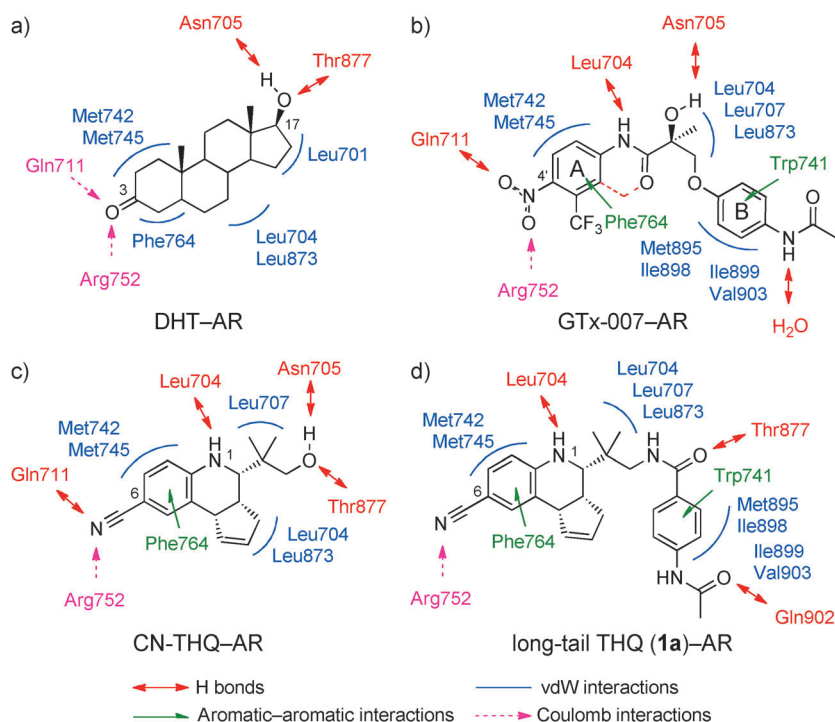
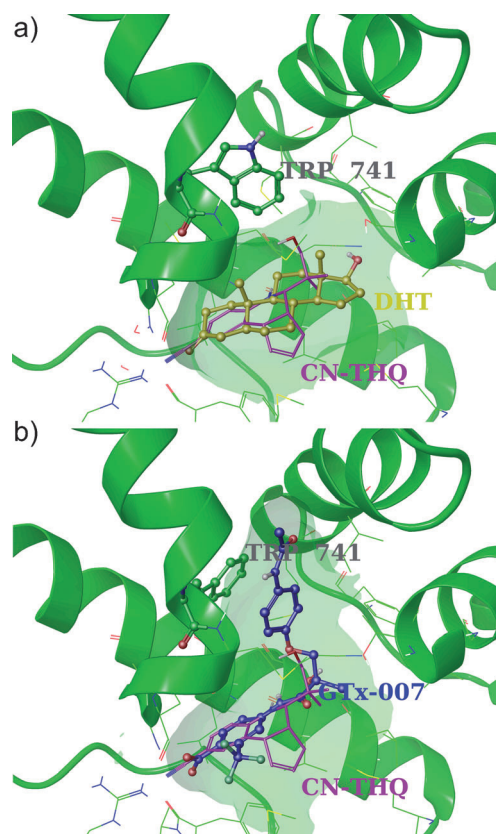


Figure 2. Ligands and their representative interaction residues in the AR. a) DHT-AR (PDB ID: 1T7T), b) GTx-007-AR (PDB ID: 3B68), c) CN-THQ-AR (assumed binding mode), and d) long-tail THQ (1a)-AR (assumed binding mode).

side chain of Gln711 and the guanidinium side chain of Arg752 in the AR. The 17-hydroxy group forms two hydrogen bonds with the amide side chain of Asn705 and the hydroxy side chain of Thr877 in the AR. Interestingly, in the case of the GTX-007-AR complex (PDB ID: 3B68),<sup>[10]</sup> the GTX-007 is stabilized by electrostatic interactions with the four hydrophilic residues Leu704, Asn705, Gln711, and Arg752, as well as a water molecule, and by vdW interactions with the surrounding hydrophobic residues Leu704, Leu707, Met742, Met745, Trp741, Phe764, Leu873, Met895, Ile898, Ile899, and Val903 (Figure 2b). The 4'-nitro group is stabilized by a hydrogen bond with the amide side chain of Gln711 and by Coulombic interactions with the guanidinium side chain of Arg752 in the AR, which is similar to the 3-carbonyl group of DHT. The amide and hydroxy groups form two hydrogen bonds with the main chain amide carbonyl of Leu704 and with the amide side chain of Asn705 in the AR, respectively. A water molecule forms hydrogen bonds with the *para*-acetamide group of the B ring of GTX-007, the side chain of His874, main chain of Gln738, and main chain of Met742 in the AR. The hydrogen bonding network of GTX-007-water-AR is considered to mediate the binding of GTX-007 to AR and to maintain the AR structure in its agonist form. Thus, the hydrogen bond that surrounds the B ring of GTX-007 is considered to play an important role in ligand binding and the agonistic activity of GTX-007. The A ring displays an edge-to-face aromatic interaction with the aromatic side chain of Phe764, and the B ring displays a  $\pi$ - $\pi$  interaction with the aromatic side chain of Trp741. In contrast, in the assumed binding mode of the CN-THQ-AR complex,<sup>[23]</sup> CN-THQ is also stabilized by electrostatic interactions with the five hydrophilic residues Leu704, Asn705, Gln711, Arg752, and Thr877, and by vdW interactions with the surrounding hydrophobic residues Leu704, Leu707, Met742, Met745, and Leu873 (Figure 2c). The 6-cyano group is stabilized by a hydrogen bond with the amide side chain of Gln711 and by Coulombic interactions with the guanidinium side chain of Arg752 in the AR. The 1-NH and the terminal hydroxy groups form three hydrogen bonds with the main chain amide carbonyl group of Leu704, with the amide side chain of Asn705, and with the hydroxy side chain of Thr877 in the AR. Thus, DHT, CN-THQ, and the nitrophenylamide moiety of GTX-007 display similar interactions with the AR and were determined to overlap within the binding pocket using protein-based superimposition (Figure 2).

Next, the shapes and volumes of the ligand binding pockets of DHT-AR and GTX-007-AR were estimated using SiteMap.<sup>[24]</sup> The pocket of the DHT-AR complex is 167 Å<sup>3</sup> (Figure 3a), and that of the GTX-007-AR complex is 199 Å<sup>3</sup> (Figure 3b). Such a large difference between the DHT-AR complex and the GTX-007-AR complex is caused by the dramatic conformational change in the side chain of Trp741 that is located in the ligand binding pocket of the GTX-007-AR complex. Thus, this large conformational change in AR induced by GTX-007 maintains the structure of the AR in its agonist form, and the B ring of GTX-007 could be placed in this newly identified binding pocket through a  $\pi$ - $\pi$  interaction with the side chain of Trp741 (Figure 3b).

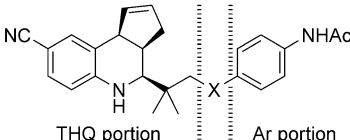


**Figure 3.** Co-crystallized structures of a) DHT-AR and b) GTX-007-AR, overlapped with the assumed binding mode of CN-THQ (DHT: yellow, GTX-007: blue, CN-THQ: purple, AR and ligand binding site surface in AR: green).

In addition to the results of the previously outlined analyses, the chemical substructure of GTX-007 was compared with the scaffold of CN-THQ. If the nitrophenylamide moiety of GTX-007 was converted into a fused ring, similar to the red dashed line in Figure 2b, then the designed compound would be considered to be very similar to the scaffold of CN-THQ. Thus, the THQ ring is a bioisostere of the nitrophenylamide moiety of GTX-007, and we considered these moieties to be interchangeable. Conversely, a bulky substituent such as a *para*-substituted aromatic group could be attached in place of the hydroxy group of CN-THQ in maintaining AR binding affinity and agonistic activity in a manner similar to that of GTX-007. Docking studies were conducted to find the most suitable linker for connecting the THQ ring with bulky groups, like a *para*-substituted aromatic ring: amide, amine, ether, and sulfone were selected as linkers, and *para*-acetamide-substituted benzyl and phenyl groups were selected as the aromatic portions.

The docking studies were performed using Glide SP mode, and the protein in the GTX-007-AR complex (PDB ID: 3B68)<sup>[10]</sup> was used as a template, because of the advantage of the aforementioned. Another advantage in using this complex is that Dalton et al. had successfully obtained GTX-007 as a SARM from structural modification of the existing nonsteroidal AR antagonist bicalutamide.<sup>[25]</sup> Concretely, the antagonist function was switched to the agonist function by changes in the cyano

**Table 1.** Docking scores,  $\Delta G_{\text{bind}}$  values, and average number of hydrogen bonds.<sup>[a]</sup>

						
Compd	X (Linker)	Docking Score	$\Delta G_{\text{bind}}^{[b]}$ [kcal mol <sup>-1</sup> ]	Hydrogen bond <sup>[c]</sup>		
				THQ	Linker	Ar
<b>1 a</b>	NHCO	−8.72	−131.4	0.7	0.4	1.0
<b>2</b>	CONH	NA	NA	NA	NA	NA
<b>3</b>	O	−8.98	−127.7	0.8	0.0	0.6
<b>4</b>	OCH <sub>2</sub>	−10.55	−138.1	0.4	0.0	0.0
<b>5</b>	NH	−9.98	−129.5	0.9	0.0	0.1
<b>6</b>	NHCH <sub>2</sub>	−10.98	−129.5	0.5	0.2	0.1
<b>7</b>	SO <sub>2</sub>	NA	NA	NA	NA	NA
<b>8</b>	SO <sub>2</sub> CH <sub>2</sub>	NA	NA	NA	NA	NA

[a] NA: no appropriated docking poses were obtained. [b] Values are the means of the calculated results of the MD trajectories using Prime MM-GBSA (1–12 ns). [c] Hydrogen bonds are the means of the calculated results of the MD trajectories using the g\_hbond module (1–12 ns).

group and sulfonyl linker of bicalutamide to the nitro group and ether linker. The results of the docking studies demonstrate that the compounds containing NHCO, ether, and amine linkers are able to dock, whereas compounds containing CONH and SO<sub>2</sub> linkers are unable to dock (Table 1). To select the best linker among the four, we performed a molecular dynamics (MD) simulation (12 ns) using GROMACS 4.5.1,<sup>[26]</sup> and then calculated the binding free energy ( $\Delta G_{\text{bind}}$ ) and average number of hydrogen bonds.  $\Delta G_{\text{bind}}$  was estimated using Prime MM-GBSA, which is based on the molecular mechanics/generalized Born surface area (MM/GBSA) method included in the Schrödinger Suite,<sup>[24]</sup> and the number of hydrogen bonds was estimated with the g\_hbond module in GROMACS.

The THQ structure was divided into three portions (THQ, linker, and aromatic (Ar)), and the number of hydrogen bonds contained in each portion were then counted (Table 1). The ether linker (OCH<sub>2</sub>) compound **4** was determined to be the best one based on the results of the  $\Delta G_{\text{bind}}$  calculations. However, we considered the amide linker (NHCO) compound **1 a** to be the best compound in terms of hydrogen bonding and synthetic accessibility, as well as the  $\Delta G_{\text{bind}}$  calculations. From the hydrogen bond analyses, the direct hydrogen bond between the *para*-acetamide group of the Ar portion of THQ and the side chain of Gln902 on H12 were considered to be indispensable in maintaining the AR structure in its agonist form (Figure 4). Additionally, as far as synthetic accessibility is concerned, the aromatic carboxylic acid was determined to be a useful component because amide linkages can easily be formed by various types of condensation reactions.

The interaction of our designed long-tail THQ derivative **1 a** with the ligand binding pocket residues of the AR is similar to the interaction between GTx-007 and AR, as we had predicted (Figure 2d). Based on the results of the MD simulation, **1 a** was determined to be stabilized in the ligand binding pocket of

the AR by electrostatic interactions with the four hydrophilic residues Leu704, Arg752, Thr877, and Gln902, and by vdW interactions with the surrounding hydrophobic residues Leu704, Leu707, Met742, Met745, Trp741, Phe764, Leu873, Met895, Ile898, Ile899, and Val903. The 6-cyano group is stabilized by Coulombic interactions with the guanidinium side chain of Arg752 in the AR. The 1-NH group and two of the carbonyl groups within the amide groups of **1 a** form three hydrogen bonds with the main chain amide carbonyl of Leu704, with the hydroxy side chain of Thr877, and with the amide side chain of Gln902 in the AR, respectively. The hydrogen bond between the *para*-acetamide group on the Ar portion of THQ and the amide side chain of Gln902 on H12 is believed to maintain the AR in its agonist form in a manner similar to the GTx-007–AR complex. Thus, this hydrogen bond is one of the key interactions that we used to design our long-tail THQ derivative. The THQ scaffold consists of an edge-to-face aromatic interaction with the aromatic side chain of Phe764,

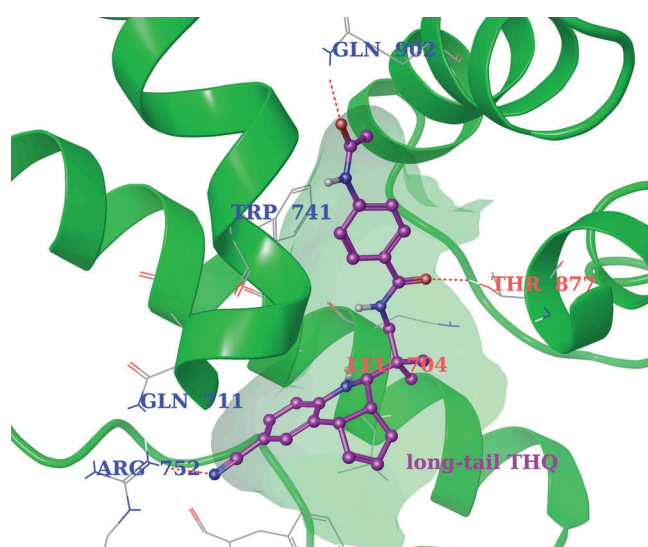


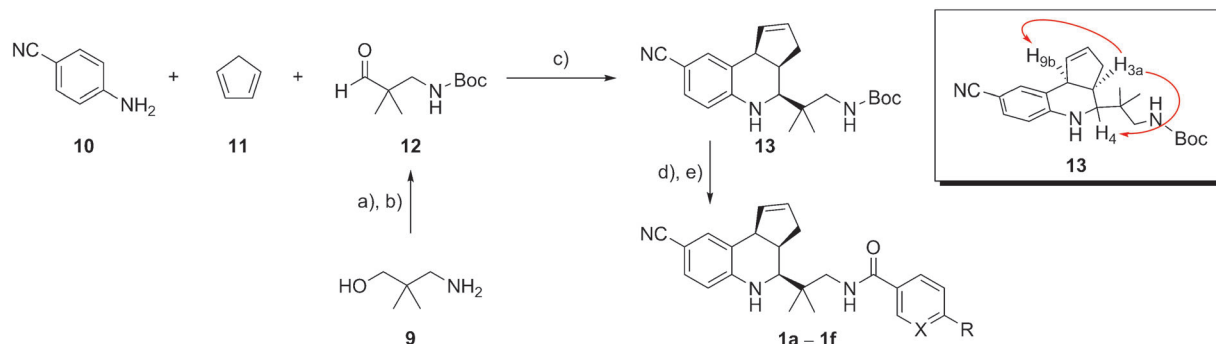
**Figure 4.** The lowest-energy binding mode of long-tail THQ **1 a** (long-tail THQ: purple, AR and ligand binding site surface in AR: green; hydrogen bond: dashed red line).

and the Ar ring of **1 a** consists of a  $\pi$ – $\pi$  interaction with the aromatic side chain of Trp741.

## Chemistry

Tricyclic THQ derivatives were obtained using Grieco three-component condensation (Scheme 1).<sup>[27]</sup> The intermediate **13** can be synthesized in a single step by treating 4-cyanoaniline **10** with cyclopentadiene **11** and *N*-Boc-3-amino-2,2-dimethylpropionaldehyde **12** in the presence of an equimolar amount of trifluoroacetic acid (TFA) in acetonitrile. The stereochemistry of **13** was assigned on the basis of coupling constants and





**Scheme 1.** Synthesis of tetrahydroquinoline derivatives **1a–f**. Reagents and conditions: a)  $\text{Boc}_2\text{O}/\text{THF}$ , RT, 3 h (100%); b)  $\text{WSCD}\cdot\text{HCl}$ ,  $\text{H}_3\text{PO}_3/\text{DMSO}$ , RT, 30 min (95%); c)  $\text{TFA}/\text{CH}_3\text{CN}$ , RT, 1 h (65%); d) 4 N  $\text{HCl}/\text{dioxane}$ ,  $60^\circ\text{C}$ , 1 h; e)  $\text{Ar}\cdot\text{COOH}$ ,  $\text{WSCD}\cdot\text{HCl}$ ,  $\text{HOBt}$ ,  $\text{NMM}/\text{DMF}$ , RT, 1–17 h (42–94%, two steps).

NOESY experiments. Saturation of proton  $\text{H}_{3a}$  in **13** gave an NOE enhancement on  $\text{H}_{9b}$  of 3.9% and  $\text{H}_4$  of 2.9%, confirming the six-membered quinoline ring and cyclopentene ring are *cis* fused and the protons  $\text{H}_{3a}$  and  $\text{H}_4$  are *cis* (Scheme 1). Alternatively, the aldehyde **12** was synthesized from the corresponding amino alcohol **9** using Boc protection followed by Moffatt oxidation. After the THQ scaffold was constructed, the Boc group of **13** was deprotected, and the appropriate aromatic carboxylic acids, *para*-substituted benzoic acids, and nicotinic acids were coupled to THQ scaffolds via amide linkages. The *para*-substituted groups were selected based on several aspects: the available potential for hydrogen bond formation, the electron density of the aromatic ring, the physicochemical properties, and so on. Acetylamino, formylamino, and trifluoromethoxy groups were selected as substituents for benzoic acid, and acetylamino, ethoxy, and chloride groups were selected for nicotinic acid. The desired compounds **1a–f** were obtained in moderate to high yields. Various calculated octanol/water partition coefficients ( $\text{clog}P$ ; 2.83–5.47) and polar surface areas (PSA; 75.9–116.8  $\text{\AA}^2$ ) were obtained based on the characteristics of the aromatic rings and their substituted functional groups (Table 2). The two physicochemical properties were estimated using QikProp.<sup>[24]</sup> By NOE experiment, we identified that the stereochemistry of **1d** is the same as **13**. Furthermore, **1a–c**, **1e**, and **1f** have the same stereochemistry as **13**, as determined by the  $^1\text{H}$  and  $^{13}\text{C}$  NMR data.

## In vitro profiles

To validate the results of our docking studies, we evaluated the binding affinities of **1a–f** and their agonistic activities on the AR (Table 2). The binding affinities of **1a–f** for rat AR ranged from 9–81 nM and are in the same range as that of our previous results.<sup>[17]</sup> Although their binding affinities were 5–40-fold weaker than that of DHT, such binding affinities are sufficient to reveal their anabolic activities in an animal model. Compound **1a** displayed particularly strong binding affinity, as predicted. We hypothesized that the predicted binding mode of **1a** would be similar to the 3D structure of GTx-007. Despite the fact that some of the compounds do not contain a potential hydrogen bonding group in their Ar portion, the compounds with similar molecular shapes also display high binding affinities. These results indicate that molecular shape is also important for high binding affinities.

The agonistic activities of the compounds in human osteoblastic (TE-85) cells were evaluated using two indices: The half-maximum effective concentration ( $\text{EC}_{50}$ ) and efficacy. The efficacy is the maximal transactivation activity of the compounds relative to that of 1000 nM DHT (100%). Compounds **1a–f** all exhibited agonistic activity ( $\text{EC}_{50}$ ) < 200 nM. These results are consistent with our predicted binding mode. In particular, the  $\text{EC}_{50}$  values of **1a** and **1d** are 5 and 1.3 nM, respectively, and their activities are 4–10-fold stronger than that of DHT. With respect to efficacy, **1a**, **1b**, and **1d** displayed higher efficacies

than those of the other compounds. However, **1b** was excluded as a candidate due to its high  $\text{EC}_{50}$  value.

The calculated physicochemical properties ( $\text{clog}P$  and PSA) were relevant with aqueous solubility and free compound ratio of plasma protein binding (PPB). In the results of in vitro ADME analyses, the above two parameters of **1d** were marginally superior to that of **1a** (Table 3). In any other common parameters, such as microsome intrinsic

**Table 2.** In vitro biological activities of the AR and calculated physicochemical properties of the THQ derivatives.

Compd	X	R	$\text{clog}P^{[a]}$	PSA [ $\text{\AA}^2$ ] <sup>[a]</sup>	$\text{IC}_{50}$ [nM] <sup>[b]</sup>	Agonistic Activity <sup>[c]</sup>	
						$\text{EC}_{50}$ [nM]	Efficacy [%]
DHT					2.0	19	100
<b>1a</b>	CH	NHAc	3.75	105.2	9.4	5	88
<b>1b</b>	CH	NHCHO	3.01	116.8	33	147	153
<b>1c</b>	CH	$\text{OCF}_3$	5.47	75.9	81	10	59
<b>1d</b>	N	NHAc	2.83	114.6	38	1.3	91
<b>1e</b>	N	OEt	4.49	89.2	38	14	54
<b>1f</b>	N	Cl	4.22	80.5	28	16	68

[a] Calculated using QikProp. [b] Binding affinities were determined by competitive binding assays with rat AR. [c] Agonistic activities were determined based on the transcriptional activities in human TE-85 cells.

**Table 3.** In vitro ADME properties of the THQ derivatives.

Compd	X	R	Solubility <sup>[a]</sup> [ $\mu\text{g mL}^{-1}$ ]	PPB [% free] <sup>[b]</sup> Human/Rat	CL <sub>int</sub> [ $\text{mL min}^{-1} \text{mg}^{-1}$ ] <sup>[c]</sup> Human/Rat	Caco-2 $P_{\text{app}}$ [ $10^{-6} \text{ cm sec}^{-1}$ ] <sup>[d]</sup> A $\rightarrow$ B/B $\rightarrow$ A	Efflux Ratio <sup>[e]</sup>
<b>1a</b>	CH	NHAc	2.1	1.3/2.5	0.05/0.01	6/7	1.2
<b>1b</b>	CH	NHCHO	2.2	4.0/51.1	0.00/0.00	29/32	1.1
<b>1c</b>	CH	OCF <sub>3</sub>	0.0	0.1/0.3	0.05/0.01	2/0	0.0
<b>1d</b>	N	NHAc	4.1	2.1/2.1	0.06/0.01	18/21	1.2
<b>1e</b>	N	OEt	0.1	2.8/5.2	0.09/0.01	27/13	0.5
<b>1f</b>	N	Cl	0.0	0.9/4.3	0.07/0.01	15/7	0.5

[a] Measured by the weight dissolved in phosphate buffer (pH 6.8). [b] Assessed by equilibrium dialysis in plasma from the appropriate species at 37 °C; free and bound concentrations were quantified by LC–MS/MS. [c] Compounds were incubated at 0.5  $\mu\text{g mL}^{-1}$  with suspended rat or human hepatocytes at 2  $\text{mg mL}^{-1}$ , and intrinsic clearance was calculated based on the rate of disappearance of the parent compound. [d] Measured permeability (A  $\rightarrow$  B/B  $\rightarrow$  A) through Caco-2 cells. [e]  $P_{\text{app}}(\text{B} \rightarrow \text{A})/P_{\text{app}}(\text{A} \rightarrow \text{B})$  in Caco-2 cells.

clearances (CL<sub>int</sub>) and Caco-2 permeability ( $P_{\text{app}}$ ), **1a** and **1d** did not clearly differ. Based on these results of such in vitro studies, we selected compound **1d** as the best compound among **1a–f**.

During the next stage of our lead evaluation process, we evaluated the receptor selectivity of **1d** for five steroid hormone receptors. The binding affinities (IC<sub>50</sub>) for each receptor were determined by calculating the competitive binding activity with each endogenous radiolabeled ligand. The endogenous ligands for each receptor were as follows: progesterone for the progesterone receptor (PR), 17 $\beta$ -estradiol for the estrogen receptor (ER), dexamethasone for the glucocorticoid receptor (GR), and aldosterone for the mineralocorticoid receptor (MR). The IC<sub>50</sub> of **1d** for each receptor was 25.8 nM for the AR, 667 nM for the PR, >50 000 nM for the GR and MR, and >500 000 nM for the ER. The IC<sub>50</sub> value of **1d** for the AR is >25-fold higher than any other steroid hormone receptor and is higher than the value we had determined in our previous studies.<sup>[17]</sup> Because compound **1d** displays sufficient receptor selectivity, we chose **1d** as a candidate for our in vivo oral administration study.

### In vivo pharmacology

The tissue selectivity of the SARMS was examined in an ovariectomized (OVX) rat model, because osteoporosis patients are mainly post-menopausal elderly women.<sup>[28]</sup> Thus, our ideal SARM should have an osteoanabolic effect and no androgenic effects in women. OVX rats were maintained without treatment for four weeks to permit bone loss. The treatment group was treated with **1d** by oral administration once daily for eight weeks. The sham-operated control group (Sham) and the OVX-operated control group (OVX-vehicle) were treated with the vehicle solution, while the positive control group was treated with DHT (10  $\text{mg kg}^{-1}$ ) by subcutaneous injection once daily for eight weeks.

Desired and/or undesired activities were evaluated using three indices. The BMD of the femur was used as an index of desirable osteoanabolic activity, while the weights of the uterus and clitoral gland (CG) were used as indices of undesirable side effects (Figure 5).<sup>[29]</sup> The uterus, which is composed of an endometrium and a myometrium, is both an estrogen- and

androgen-responsive tissue, whereas the CG is one of the secretory glands and is an androgen-responsive tissue. Thus, increases in the uterus weight could induce endometriosis or uterine fibroids, whereas increases in the CG weight could induce acne or oily skin.

In the OVX-vehicle group, femoral BMD and uterus weight were significantly decreased, whereas the CG weight was influenced far less. In the **1d** oral administration group, these parameters increased in a dose-dependent manner. Femoral BMD increased gradually and reached 99% of the sham group at a dose of 30  $\text{mg kg}^{-1}$  for **1d**. Uterus weight also increased gradually. However, uterus weight reached 42% of the sham group at a dose of 30  $\text{mg kg}^{-1}$  for **1d**. The CG weight was increased to the sham level (99%) at a dose of 3  $\text{mg kg}^{-1}$  and exceeded the sham level at doses of 10 and 30  $\text{mg kg}^{-1}$  of **1d** (124 and 147%, respectively). In the DHT administration group, the femoral BMD was increased to the sham level (97%), and the uterus weight was increased to 70% of the sham group. Surprisingly, the CG weight was remarkably increased to 289% of the sham group.

Next, the effects of **1d** on these three parameters were compared with DHT. Even at a dose of 3  $\text{mg kg}^{-1}$  of **1d**, femoral BMD reached the same level as DHT. In contrast, at doses of 3, 10, and 30  $\text{mg kg}^{-1}$  of **1d**, the uterus weights were 39, 54, and 60% of DHT, and the CG weights were 34, 43, and 51% of DHT. Based on these results, **1d** was considered to be a SARM with osteoanabolic effects equal to that of DHT, yet with fewer virilizing effects. However, the uterine and CG weights were significantly increased relative to the OVX-vehicle. These effects should be decreased prior to clinical use, and further optimization is required to develop an ideal SARM.

### Conclusions

The lead evaluation process of our THQ derivatives as SARMS was described. THQ is a validated scaffold that possesses osteoanabolic tissue selectivity, so we adapted the strategy of switching from the antagonist activity of THQ to the agonist function, and optimized THQ for use as an orally available SARM. From the viewpoints of the computational study and synthetic accessibility, we designed and synthesized several CN-THQ compounds that possess *para*-substituted aromatic

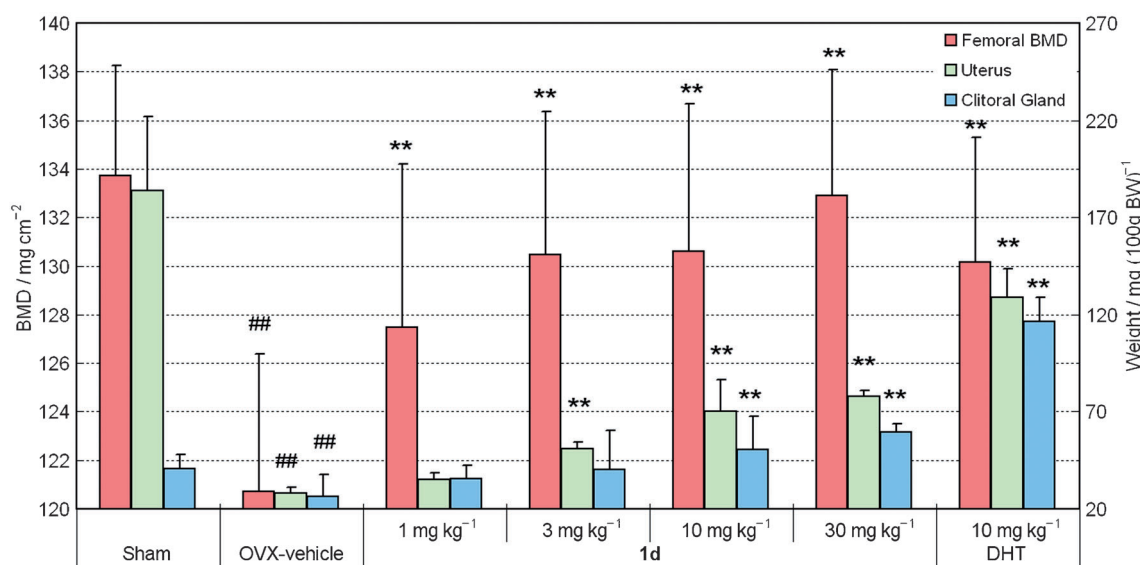


**Figure 5.** Comparison of the desired osteoanabolic effect on the femoral BMD and the undesired side effects on the uterine and CG of **1d** and DHT in OVX rats (<sup>##</sup> $p < 0.01$  vs. Sham, <sup>\*\*</sup> $p < 0.01$  vs. OVX-vehicle); BW: body weight.

rings connected via amide linkers. The long-tail THQ derivative **1d** was determined to be a promising orally available compound based on the results of in vitro studies. The in vivo tissue selectivity for bone was revealed based on the fact that **1d** clearly dissociates from DHT in OVX rats following oral administration. Thus, as predicted, this compound was determined to have an attractive SARM profile. However, the increased uterus and CG weights induced by **1d** must be decreased to the levels observed in the OVX-vehicle. Therefore, further optimization processes will be required to decrease virilizing effects to obtain ideal SARMS.

## Experimental Section

### Computational study

**Ligand and AR preparation:** Hydrogen atoms and charges were added to the 2D structures of the ligands, and then converted into their corresponding 3D structures using LigPrep.<sup>[24]</sup> The protein structure of the AR (PDB ID: 3B68) was obtained from the Protein Data Bank.<sup>[10]</sup> All of the residues were protonated, and the protein structures were refined to relieve steric clashes with a restrained minimization of the OPLS2005 force field until a final RMSD of 0.030 Å was reached with respect to the input protein coordinates using the Protein Preparation Wizard, which is included in the Schrödinger Suite 2012.<sup>[24]</sup>

**Docking:** The docking studies were performed using Glide.<sup>[24]</sup> The energy grid was built from the protein structures and was prepared as described above. An atomic van der Waals radius scaling factor, a partial atomic charge, and the sizes of the enclosing and bounding boxes were used as the default values. The SP docking protocol (ligands were docked flexibly, the sampling of ring conformations was included, and nonplanar amide conformations were penalized) was performed to be energy minimized on the OPLS-AA non-bonded interaction with the grid, and each term (the Coulombic term ( $\Delta E_{\text{coul}}$ ) and the vdW term ( $\Delta E_{\text{vdW}}$ )) was decomposed for each residue.

**MD simulations:** MD simulations were performed using the GRO-MACS 4.5.1 package<sup>[26]</sup> with AMBER ff03 force field parameters<sup>[30]</sup> and periodic boundary conditions. Protein–ligand complexes were solvated in  $91 \times 84 \times 91$  Å<sup>3</sup> boxes at a density of  $1 \text{ g cm}^{-3}$ , with the TIP3P water model.<sup>[31]</sup> An appropriate number of counterions ( $\text{Cl}^-$ ) were added in the box to neutralize the systems. The temperature control was set using the Berendsen thermostat at 300 K, and pressure coupling was implemented using the Berendsen barostat with a constant pressure of 1 atm.<sup>[32]</sup> Non-bonded interactions were cut off at 10 Å with updates at every five steps, and the particle mesh Ewald (PME) method was used for the long-range electrostatic interactions.<sup>[33,34]</sup> The LINCS procedure for covalent bond constraints was used.<sup>[35]</sup> MD simulations were performed using a constant-NPT ensemble. The energy of these complexes was minimized using the steepest descent approach and heating the system for 20 ps using the NVT ensemble. An equilibration step of 1 ns was followed by a production run of 11 ns, with a time step of 1.0 fs, and trajectories were collected every 10 ps. The total simulation time was 12 ns for each complex for the binding mode selection. Each analysis was performed using the GROMACS modules and MD trajectories (1–12 ns).<sup>[26]</sup> Binding free energies ( $\Delta G_{\text{bind}}$ ) were calculated using Prime MM-GBSA, which is included in the Schrödinger Suite<sup>[24]</sup> and MD trajectories (1–12 ns).

### Chemistry

**General:** All starting materials and reagents were purchased from commercial suppliers and were used without further purification. <sup>1</sup>H and <sup>13</sup>C NMR spectra were recorded using a JEOL JNM-ECA 400 MHz spectrometer in solution in the deuterated solvent ( $\text{CDCl}_3$ ); chemical shifts ( $\delta$ ) are expressed in parts per million relative to tetramethylsilane, which was used as a reference. High-resolution mass spectrometry (HRMS) analyses were performed on a Thermo Scientific Exactive Mass Spectrometer in positive or negative electrospray ionization mode operating at 25000 resolution.

**N-(tert-Butyloxycarbonyl)-3-amino-2,2-dimethylpropionaldehyde (12):** Boc<sub>2</sub>O (59 g, 314 mmol) was added to a solution of 3-amino-2,2-dimethylpropanol **9** (25 g, 242 mmol) in anhydrous THF

(120 mL) at 0 °C. The mixture was stirred at room temperature for 3 h. The mixture was evaporated, and the residue was diluted using EtOAc (100 mL) and H<sub>2</sub>O (30 mL). The organic layer was separated and washed with brine (30 mL), dried over Na<sub>2</sub>SO<sub>4</sub>, and evaporated. The desired *N*-Boc-protected amino propanol was obtained as an intermediate (49.6 g, >100%). A portion of the *N*-Boc-protected aminopropanol (5.0 g, 24.6 mmol) and phosphoric acid (0.65 mL, 12.5 mmol) were dissolved in DMSO (50 mL). Water-soluble carbodiimide hydrochloride (WSCD-HCl; 14 g, 74.0 mmol) was added and stirred at room temperature for 30 min. The mixture was poured into cold water (50 mL) and extracted with EtOAc (100 mL×3). The combined organic layers were washed with H<sub>2</sub>O (50 mL) and brine (50 mL), dried over Na<sub>2</sub>SO<sub>4</sub>, and evaporated to generate the desired product (4.68 g, 95%). <sup>1</sup>H NMR (400 MHz, CDCl<sub>3</sub>): δ=1.09 (s, 6H), 1.42 (s, 9H), 2.61 (s, 2H), 4.83 (brs, 1H), 9.45 ppm (s, 1H).

***N*-(*tert*-Butyloxycarbonyl)-2-(8-cyano-3a,4,5,9b-tetrahydro-3H-cyclopenta[c]quinolin-4-yl)-2-methyl propylamine (13):** *N*-Boc-protected aldehyde **12** (2.0 g, 10.0 mmol) was added to a mixture of 4-cyanoaniline **10** (1.2 g, 10.0 mmol), freshly prepared cyclopentadiene **11** (1.7 mL, 20.0 mmol), and TFA (0.88 mL, 11.0 mmol) in CH<sub>3</sub>CN (5 mL) at 0 °C. The mixture was stirred at room temperature for 1 h. The precipitate was filtered, washed with Et<sub>2</sub>O, dried under reduced pressure, and the desired product was then obtained (2.4 g, 65%). <sup>1</sup>H NMR (400 MHz, CDCl<sub>3</sub>): δ=0.99 (s, 3H), 1.02 (s, 3H), 1.34 (s, 9H), 2.26 (dd, *J*=8.24, 14.65 Hz, 1H), 2.47–2.54 (m, 1H), 2.82–2.90 (m, 1H), 3.27 (s, 1H), 3.39 (dd, *J*=8.24, 14.20 Hz, 1H), 3.93 (d, *J*=8.24 Hz, 1H), 4.51 (brs, 1H), 4.70 (brs, 1H), 5.74–5.76 (m, 1H), 5.86–5.88 (m, 1H), 6.60 (d, *J*=8.24 Hz, 1H), 7.17–7.22 ppm (m, 1H); HRMS-ESI *m/z* [*M*+H]<sup>+</sup> calcd for C<sub>22</sub>H<sub>29</sub>N<sub>3</sub>O<sub>2</sub>: 367.2260, found: 368.2331.

**General amide formation procedure using aromatic carboxylic acids:** Preparation of 6-acetamido-*N*-(2-(8-cyano-3a,4,5,9b-tetrahydro-3H-cyclopenta[c]quinolin-4-yl)-2-methylpropyl)nicotinamide (**1d**): A solution of HCl in dioxane (4N, 136 mL) was added to a stirred solution of *N*-Boc-protected tetrahydroquinoline **13** (40 g, 109 mmol) in anhydrous THF (100 mL) at room temperature. The resulting mixture was then stirred at 60 °C for 1 h. The suspension was diluted with EtOAc (50 mL) and poured into 5N NaCl(aq) (50 mL). The organic layer was separated and extracted with EtOAc (100 mL×3). The combined organic layers were washed with brine (50 mL), dried over Na<sub>2</sub>SO<sub>4</sub>, and evaporated. The desired amine was obtained as an intermediate. The *N*-Boc-deprotected tetrahydroquinoline in DMF (100 mL) was added to the mixture of 6-acetamidonicotinic acid (29 g, 163 mmol), WSCD-HCl (31 g, 163 mmol), 1-hydroxybenzotriazole (HOBt; 22 g, 163 mmol), and *N*-methylmorpholine (NMM; 29 mL, 163 mmol) in DMF (200 mL) at 0 °C. The mixture was stirred at room temperature for 3 h. The mixture was quenched with H<sub>2</sub>O (50 mL), extracted with EtOAc (100 mL×3), washed with brine (50 mL), dried over Na<sub>2</sub>SO<sub>4</sub>, and evaporated. The residue was purified by column chromatography (hexane/EtOAc 1:4) followed by charcoal treatment. The title compound was obtained as a white solid (27.4 g, 59%). <sup>1</sup>H NMR (400 MHz, CDCl<sub>3</sub>): δ=1.09 (s, 3H), 1.14 (s, 3H), 2.23 (s, 3H), 2.30 (dd, *J*=8.24, 14.20 Hz, 1H), 2.46–2.56 (m, 1H), 2.84–2.94 (m, 1H), 3.22 (dd, *J*=5.95, 14.20 Hz, 1H), 3.32 (d, *J*=1.37 Hz, 1H), 3.78 (dd, *J*=7.33, 14.20 Hz, 1H), 3.90 (d, *J*=8.24 Hz, 1H), 4.57 (s, 1H), 5.77 (d, *J*=5.04 Hz, 1H), 5.87–5.92 (m, 1H), 6.45 (t, *J*=6.41 Hz, 1H), 6.65 (d, *J*=8.24 Hz, 1H), 7.17–7.22 (m, 2H), 8.01 (dd, *J*=2.29, 8.70 Hz, 2H), 8.21 (s, 1H), 8.24 (d, *J*=8.70 Hz, 1H), 8.64 ppm (d, *J*=2.29 Hz, 1H); <sup>13</sup>C NMR (100 MHz, CDCl<sub>3</sub>): δ=22.5, 25.1, 32.5, 38.3, 40.9, 47.4, 48.5, 58.4, 67.3, 77.0, 77.3, 77.6, 100.6, 113.2, 116.4, 120.7, 125.8, 130.6,

132.0, 133.1, 137.4, 147.5, 153.8, 165.9, 169.3 ppm; HRMS-ESI *m/z* [*M*+H]<sup>+</sup> calcd for C<sub>25</sub>H<sub>27</sub>N<sub>5</sub>O<sub>2</sub>: 429.2165, found: 430.2236.

**4-Acetamido-*N*-(2-(8-cyano-3a,4,5,9b-tetrahydro-3H-cyclopenta[c]quinolin-4-yl)-2-methylpropyl)benzamide (1a):** Compound **1a** was prepared by following the same method used to generate compound **1d**. 4-Acetamidobenzoic acid was used as an aromatic carboxylic acid (22 mg, 94%). <sup>1</sup>H NMR (400 MHz, CDCl<sub>3</sub>): δ=1.03 (s, 3H), 1.13 (s, 3H), 2.19 (s, 3H), 2.29 (dd, *J*=8.24, 14.20 Hz, 1H), 2.48–2.55 (m, 1H), 2.88 (q, *J*=8.24 Hz, 1H), 3.17 (dd, *J*=5.95, 14.65 Hz, 1H), 3.30 (d, *J*=1.83 Hz, 1H), 3.79 (dd, *J*=7.33, 14.65 Hz, 1H), 3.89 (d, *J*=8.24 Hz, 1H), 4.66 (brs, 1H), 5.76 (d, *J*=5.04 Hz, 1H), 5.86–5.91 (m, 1H), 6.44 (t, *J*=6.41 Hz, 1H), 6.65 (d, *J*=8.70 Hz, 1H), 7.15–7.20 (m, 2H), 7.55 (d, *J*=8.70 Hz, 2H), 7.64 (s, 1H), 7.65 ppm (d, *J*=8.70 Hz, 2H); <sup>13</sup>C NMR (100 MHz, CDCl<sub>3</sub>): δ=22.4, 24.5, 31.2, 32.6, 38.3, 40.9, 47.4, 48.6, 58.4, 77.3, 77.5, 77.6, 116.5, 119.5, 120.7, 126.3, 128.2, 130.6, 132.0, 133.1, 133.5, 141.3, 141.9, 150.4, 167.5, 180.0 ppm; HRMS-ESI *m/z* [*M*+H]<sup>+</sup> calcd for C<sub>26</sub>H<sub>28</sub>N<sub>4</sub>O<sub>2</sub>: 428.2212, found: 429.2283.

***N*-(2-(8-Cyano-3a,4,5,9b-tetrahydro-3H-cyclopenta[c]quinolin-4-yl)-2-methylpropyl)-4-formamidebenzamide (1b):** Compound **1b** was prepared by following the same method used to generate compound **1d**. 4-Formamidobenzoic acid was used as an aromatic carboxylic acid (1.20 g, 59%). <sup>1</sup>H NMR (400 MHz, CDCl<sub>3</sub>): δ=1.08 (s, 3H), 1.13 (s, 3H), 2.30 (dd, *J*=8.24, 14.20 Hz, 1H), 2.46–2.56 (m, 1H), 2.83–2.93 (m, 1H), 3.17 (dd, *J*=5.50, 14.20 Hz, 1H), 3.29 (d, *J*=1.83 Hz, 1H), 3.80 (dd, *J*=7.79, 14.20 Hz, 1H), 3.89 (d, *J*=7.79 Hz, 1H), 4.66 (s, 1H), 5.77 (d, *J*=5.50 Hz, 1H), 5.86–5.91 (m, 1H), 6.40 (t, *J*=6.87 Hz, 1H), 6.65 (d, *J*=8.24 Hz, 1H), 7.16–7.21 (m, 2H), 7.55 (s, 1H), 7.56 (d, *J*=8.70 Hz, 2H), 7.66 ppm (d, *J*=8.70 Hz, 2H); <sup>13</sup>C NMR (100 MHz, CDCl<sub>3</sub>): δ=22.4, 24.5, 32.6, 38.3, 40.9, 47.4, 48.6, 58.3, 77.0, 77.3, 77.6, 100.2, 116.5, 119.5, 120.9, 126.3, 128.2, 129.6, 130.6, 132.1, 133.1, 141.5, 150.5, 167.9, 169.3 ppm; HRMS-ESI *m/z* [*M*+H]<sup>+</sup> calcd for C<sub>25</sub>H<sub>26</sub>N<sub>4</sub>O<sub>2</sub>: 414.2056, found: 415.2102.

***N*-(2-(8-Cyano-3a,4,5,9b-tetrahydro-3H-cyclopenta[c]quinolin-4-yl)-2-methylpropyl)-4-(trifluoromethoxy)benzamide (1c):** Compound **1c** was prepared by following the same method used to generate compound **1d**. 4-(Trifluoromethoxy)benzoic acid was used as an aromatic carboxylic acid (31.0 g, 82%). <sup>1</sup>H NMR (CDCl<sub>3</sub>): δ=1.09 (s, 3H), 1.14 (s, 3H), 2.31 (dd, *J*=8.24, 14.20 Hz, 1H), 2.47–2.51 (m, 1H), 2.89 (q, *J*=8.24 Hz, 1H), 3.21 (dd, *J*=5.50, 14.20 Hz, 1H), 3.30 (d, *J*=1.83 Hz, 1H), 3.79 (dd, *J*=7.33, 14.20 Hz, 1H), 3.90 (d, *J*=8.24 Hz, 1H), 4.57 (s, 1H), 5.77 (d, *J*=5.04 Hz, 1H), 5.87–5.92 (m, 1H), 6.36 (t, *J*=6.41 Hz, 1H), 6.66 (d, *J*=8.24 Hz, 1H), 7.19 (s, 1H), 7.21 (dd, *J*=1.83, 8.24 Hz, 1H), 7.24–7.28 (m, 2H), 7.72–7.78 ppm (m, 2H); <sup>13</sup>C NMR (100 MHz, CDCl<sub>3</sub>): δ=22.5, 24.4, 32.5, 38.3, 40.9, 47.4, 48.6, 58.4, 77.0, 77.3, 77.6, 100.7, 116.5, 120.7, 121.0, 126.3, 129.1, 130.6, 132.0, 132.8, 133.1, 133.5, 150.3, 151.9, 166.9 ppm; HRMS-ESI *m/z* [*M*+H]<sup>+</sup> calcd for C<sub>25</sub>H<sub>24</sub>F<sub>3</sub>N<sub>5</sub>O<sub>2</sub>: 455.1821, found: 456.1891.

***N*-(2-(8-Cyano-3a,4,5,9b-tetrahydro-3H-cyclopenta[c]quinolin-4-yl)-2-methylpropyl)-6-ethoxynicotinamide (1e):** Compound **1e** was prepared by following the same method used to generate compound **1d**. 6-Ethoxynicotinic acid was used as an aromatic carboxylic acid (6.46 g, 71%). <sup>1</sup>H NMR (400 MHz, CDCl<sub>3</sub>): δ=1.09 (s, 3H), 1.14 (s, 3H), 2.31 (dd, *J*=8.24, 14.20 Hz, 1H), 2.46–2.56 (m, 1H), 2.89 (q, *J*=8.24 Hz, 1H), 3.22 (dd, *J*=5.50, 14.20 Hz, 1H), 3.31 (d, *J*=1.89 Hz, 1H), 3.78 (dd, *J*=7.33, 14.20 Hz, 1H), 3.90 (d, *J*=8.24 Hz, 1H), 4.57 (s, 1H), 5.74–5.80 (m, 1H), 5.87–5.93 (m, 1H), 6.41 (t, *J*=6.40 Hz, 1H), 6.65 (d, *J*=8.24 Hz, 1H), 7.17–7.23 (m, 2H), 8.00 (dd, *J*=2.29, 8.70 Hz, 1H), 8.24 (d, *J*=8.70 Hz, 1H), 8.64 ppm (d, *J*=2.29 Hz, 1H); <sup>13</sup>C NMR (100 MHz, CDCl<sub>3</sub>): δ=14.9, 22.5, 24.3,



32.5, 38.2, 40.9, 47.3, 48.4, 58.3, 77.0, 77.3, 77.6, 100.8, 112.7, 116.5, 120.1, 126.3, 130.6, 132.0, 133.0, 133.6, 135.6, 141.3, 150.2, 164.6 ppm; HRMS-ESI  $m/z$   $[M+H]^+$  calcd for  $C_{25}H_{28}N_4O_2$ : 416.2212, found: 417.2282.

**6-Chloro-N-(2-(8-cyano-3a,4,5,9b-tetrahydro-3H-cyclopenta[c]quinolin-4-yl)-2-methylpropyl)nicotinamide (1 f):** Compound **1 f** was prepared by following the same method used to generate compound **1 d**. 6-Chloronicotinic acid was used as an aromatic carboxylic acid (292 mg, 88 %).  $^1H$  NMR (400 MHz,  $CDCl_3$ ):  $\delta$  = 1.07 (s, 3H), 1.12 (s, 3H), 1.36 (t,  $J$  = 7.33 Hz, 3H), 2.24–2.35 (m, 1H), 2.44–2.57 (m, 1H), 2.82–2.92 (m, 1H), 3.17 (dd,  $J$  = 5.95, 14.20 Hz, 1H), 3.30 (m, 1H), 3.74 (dd,  $J$  = 7.79, 14.20 Hz, 1H), 4.01 (q,  $J$  = 7.33 Hz, 2H), 4.58 (s, 1H), 5.75–5.82 (m, 1H), 5.87–5.94 (m, 1H), 6.32 (t,  $J$  = 6.41 Hz, 1H), 6.51 (d,  $J$  = 9.16 Hz, 1H), 6.64 (d,  $J$  = 8.24 Hz, 1H), 7.16–7.22 (m, 1H), 7.18 (s, 1H), 7.52 (dd,  $J$  = 2.75, 9.62 Hz, 2H), 8.07 ppm (d,  $J$  = 2.75 Hz, 1H);  $^{13}C$  NMR (100 MHz,  $CDCl_3$ ):  $\delta$  = 22.6, 24.3, 32.5, 38.3, 40.9, 47.4, 48.5, 58.5, 77.0, 77.3, 77.6, 100.8, 116.5, 120.6, 124.8, 129.0, 130.6, 132.0, 133.6, 138.3, 148.0, 150.1, 165.3 ppm; HRMS-ESI  $m/z$   $[M+H]^+$  calcd for  $C_{23}H_{23}ClN_4O_2$ : 406.1560, found: 407.1632.

## Biology

**In vitro assays:** The in vitro binding affinity for the AR was measured by competitive binding assay with the crude rat AR protein fraction, which was prepared from the prostates of 11-week-old male rats that had been castrated three days prior. Specific binding was defined as the difference between the binding of radiolabeled ligands in the presence (nonspecific binding) and absence (total binding) of excess unlabeled ligands. Half-maximal inhibitory concentration ( $IC_{50}$ ) values were determined from a nonlinear regression analysis of the competitive binding curve. The in vitro agonistic activity was measured using an AR transactivation assay with the human TE-85 osteosarcoma cell line that had been transfected with human AR and a luciferase reporter gene. The luciferase activity induced by 1000 nM DHT was set at 100% and used as a reference. Half-maximal effective concentration ( $EC_{50}$ ) values were determined from a nonlinear regression analysis of the dose–response curve.

**In vivo pharmacology:** The tissue-selective activity of the compounds was examined using a post-menopausal rat osteoporosis model. Twelve-week-old SD rats were bilaterally OVX or sham-operated. All animals were maintained without treatment for four weeks to permit bone loss and were then treated with the compounds once daily for eight weeks. Compound **1 d** was orally administered once daily in a volume of 5 mL kg<sup>−1</sup> body weight (BW). DHT was injected subcutaneously once daily in a volume of 1 mL kg<sup>−1</sup> BW. After eight weeks of treatment, the uterus and CG of each mouse were excised and weighed immediately. The femoral BMD was measured using dual-energy X-ray absorptiometry with a bone mineral analyzer (DCS-600EX-IIIR; Aloka, Tokyo, Japan). The experimental protocol was approved by the Institutional Animal Care and Use Committee at Kaken Pharmaceutical Co. Ltd.

## Acknowledgements

The authors thank Dr. Hiroaki Nejishima, Sayuri Kataoka, Dr. Hirohide Ishige, and Dr. Kiyoshi Inoguchi (Kaken Pharmaceutical) for their support.

**Keywords:** androgen receptors • docking • selective androgen receptor modulators • osteoanabolic activity • tetrahydroquinolines

- [1] *Osteoporosis Prevention, Diagnosis, and Therapy*, NIH Consensus Statement **2000**, 17, 1–36.
- [2] A. Schmidt, S. Harada, G. A. Rodan, *Principles of Bone Biology* (Eds.: J. P. Bilezikian, L. G. Raisz, G. R. Rodan), Academic Press, San Diego, **1999**, Ch. 81, pp. 1125–1134.
- [3] R. M. Neer, C. D. Arnaud, J. R. Zanchetta, R. Prince, G. A. Gaich, J. Y. Reingster, A. B. Hodsman, E. F. Eriksen, S. Ish-Shalom, H. K. Genant, O. Wang, B. H. Mitlak, *N. Engl. J. Med.* **2001**, 344, 1434–1441.
- [4] J. Rosen, A. Negro-Vilar, *J. Musculoskeletal Neuronal Interact.* **2002**, 2, 222–224.
- [5] M. L. Mohler, C. E. Bohl, A. Jones, C. C. Coss, R. Narayanan, Y. He, D. J. Hwang, J. T. Dalton, D. D. Miller, *J. Med. Chem.* **2009**, 52, 3597–3617.
- [6] W. Gao, C. E. Bohl, J. T. Dalton, *Chem. Rev.* **2005**, 105, 3352–3370.
- [7] R. Narayanan, M. L. Mohler, C. E. Bohl, D. D. Miller, J. T. Dalton, *Nucl. Recept. Signaling* **2008**, 6, e010.
- [8] R. V. Weatherman, R. J. Fletterick, T. S. Scanlan, *Annu. Rev. Biochem.* **1999**, 68, 559–581.
- [9] C. E. Bohl, D. D. Miller, J. Chen, C. E. Bell, J. T. Dalton, *J. Biol. Chem.* **2005**, 280, 37747–37754.
- [10] C. E. Bohl, Z. Wu, J. Chen, M. L. Mohler, J. Yang, D. J. Hwang, S. Mustafa, D. D. Miller, C. E. Bell, J. T. Dalton, *Bioorg. Med. Chem. Lett.* **2008**, 18, 5567–5570.
- [11] F. Wang, X. Q. Liu, H. Li, K. N. Liang, J. N. Miner, M. Hong, E. A. Kallel, A. van Oeveren, L. Zhi, T. Jiang, *Acta. Crystallogr. Sect. F* **2006**, 62, 1067–1071.
- [12] A. A. Nirschl, Y. Zou, S. R. Krystek, Jr., J. C. Sutton, L. M. Simpkins, J. A. Lupisella, J. E. Kuhns, R. Seethala, R. Golla, P. G. Sleph, B. C. Beehler, G. J. Grover, D. Egan, A. Fura, V. P. Vyas, Y. X. Li, J. S. Sack, K. F. Kish, Y. An, J. A. Bryson, J. Z. Gougoutas, J. DiMarco, R. Zahler, J. Ostrowski, L. G. Hamann, *J. Med. Chem.* **2009**, 52, 2794–2798.
- [13] F. Nique, S. Hebbe, N. Triballeau, C. Peixoto, J. M. Lefrançois, H. Jary, L. Alvey, M. Manioc, C. Housseman, H. Klaassen, K. Van Beeck, D. Guédin, F. Namour, D. Minet, E. Van der Aar, J. Feyen, S. Fletcher, R. Blanqué, C. Robin-Jagerschmidt, P. Deprez, *J. Med. Chem.* **2012**, 55, 8236–8247.
- [14] J. Ostrowski, J. E. Kuhns, J. A. Lupisella, M. C. Manfredi, B. C. Beehler, S. R. Krystek, Jr., Y. Bi, C. Sun, R. Seethala, R. Golla, P. G. Sleph, A. Fura, Y. An, K. F. Kish, J. S. Sack, K. A. Mookhtiar, G. J. Grover, L. G. Hamann, *Endocrinology* **2007**, 148, 4–12.
- [15] J. D. Kearbey, W. Gao, R. Narayanan, S. J. Fisher, D. Wu, D. D. Miller, J. T. Dalton, *Pharm. Res.* **2007**, 24, 328–335.
- [16] J. N. Miner, W. Chang, M. C. Chapman, P. D. Finn, M. H. Hong, F. J. López, K. B. Marschke, J. Rosen, W. Schrader, R. Turner, A. van Oeveren, H. Viveros, L. Zhi, A. Negro-Vilar, *Endocrinology* **2007**, 148, 363–373.
- [17] N. Nagata, M. Miyakawa, S. Amano, K. Furuya, N. Yamamoto, K. Inoguchi, *Bioorg. Med. Chem. Lett.* **2011**, 21, 1744–1747.
- [18] N. Nagata, M. Miyakawa, S. Amano, K. Furuya, N. Yamamoto, H. Nejishima, K. Inoguchi, *Bioorg. Med. Chem. Lett.* **2011**, 21, 6310–6313.
- [19] K. Hanada, K. Furuya, N. Yamamoto, H. Nejishima, K. Ichikawa, T. Nakamura, M. Miyakawa, S. Amano, Y. Sumita, N. Oguro, *Biol. Pharm. Bull.* **2003**, 26, 1563–1569.
- [20] F. Nique, S. Hebbe, C. Peixoto, D. Annot, J. M. Lefrançois, E. Duval, L. Michoux, N. Triballeau, J. M. Lemoullec, P. Mollat, M. Thauvin, T. Prangé, D. Minet, P. Clément-Lacroix, C. Robin-Jagerschmidt, D. Fleury, D. Guédin, P. Deprez, *J. Med. Chem.* **2012**, 55, 8225–8235.
- [21] J. Kazius, R. McGuire, R. Bursi, *J. Med. Chem.* **2005**, 48, 312–320.
- [22] N. Nagata, K. Kawai, I. Nakanishi, *J. Chem. Inf. Model.* **2012**, 52, 2257–2264.
- [23] E. Hur, S. J. Pfaff, E. S. Payne, H. Grøn, B. M. Buehrer, R. J. Fletterick, *PLoS Biol.* **2004**, 2, 1303–1312.
- [24] Schrödinger Suite 2012, Schrödinger LLC, New York, NY (USA), **2012**: Maestro v. 9.3, SiteMap v. 2.6, Glide v. 5.8, Prime MM-GBSA v. 2.0, QikProp v. 3.5, LigPrep v. 2.5.
- [25] a) J. T. Dalton, A. Mukherjee, Z. Zhu, L. Kirkovsky, D. D. Miller, *Biochem. Biophys. Res. Commun.* **1998**, 244, 1–4; b) C. A. Marhefka, W. Gao, K. Chung, J. Kim, Y. He, D. Yin, C. E. Bohl, J. T. Dalton, D. D. Miller, *J. Med.*

- Chem.* **2004**, *47*, 993–998; c) J. Kim, D. Wu, D. J. Hwang, D. D. Miller, J. T. Dalton, *J. Pharmacol. Exp. Ther.* **2005**, *315*, 230–239.
- [26] a) H. J. C. Berendsen, D. van der Spoel, R. van Drunen, *Comput. Phys. Commun.* **1995**, *91*, 43–57; b) B. Hess, C. Kutzner, D. van der Spoel, E. Lindahl, *J. Chem. Theory Comput.* **2008**, *4*, 435–447.
- [27] P. A. Grieco, A. Bahsas, *Tetrahedron Lett.* **1988**, *29*, 5855–5858.
- [28] X. Zhang, Z. Sui, *Expert Opin. Drug Discovery* **2013**, *8*, 191–218.
- [29] K. Furuya, N. Yamamoto, Y. Ohyabu, A. Makino, T. Morikyu, H. Ishige, K. Kuzutani, Y. Endo, *Biol. Pharm. Bull.* **2012**, *35*, 1096–1104.
- [30] J. Wang, R. M. Wolf, J. W. Caldwell, P. A. Kollman, D. A. Case, *J. Comput. Chem.* **2004**, *25*, 1157–1174.
- [31] W. L. Jorgensen, J. Chandrasekhar, J. D. Madura, R. W. Impey, M. L. Klein, *J. Chem. Phys.* **1983**, *79*, 926–935.
- [32] H. J. C. Berendsen, P. J. M. Postma, W. F. van Gunsteren, A. DiNola, J. R. Haak, *J. Chem. Phys.* **1984**, *81*, 3684–3690.
- [33] T. Darden, D. York, L. Pedersen, *J. Chem. Phys.* **1993**, *98*, 10089–10092.
- [34] U. Essmann, L. Perera, M. L. Berkowitz, T. Darden, H. Lee, L. G. Pedersen, *J. Chem. Phys.* **1995**, *103*, 8577–8593.
- [35] B. Hess, H. Bekker, H. J. C. Berendsen, J. G. E. M. Fraaije, *J. Comput. Chem.* **1997**, *18*, 1463–1472.

---

Received: August 29, 2013

Revised: October 24, 2013

Published online on November 22, 2013